Efficiency Optimized Power Sharing Algorithm for Modular Battery Energy Storage Systems

Bortecene Yildirim, Mohammed A. Elgendy, Andrew Smith, and Volker Pickert

Abstract**-- Modular Battery Energy Storage systems (MBESSs) enable the use of lower-rated voltage converters and battery modules, and simpler battery management systems. They also improve the system's reliability and allow flexible power sharing amongst different modules. This paper proposes a power-sharing algorithm which maximizes the energy conversion efficiency of this battery energy storage system, considering state of charge (SoC) balancing and battery lifespan. Real time optimum power sharing is undertaken based on a simple look-up table, whose data was generated via off-line Genetic Algorithm optimization considering the converter's efficiency map. To demonstrate the proposed algorithms effectiveness, a six-module prototype system was constructed, each comprising of a half-bridge converter and a 10 Ah, 12.8 V, LiFePo4 battery. System testing occurred at different battery power levels in both charging and discharging modes, using the proposed efficiency optimized power-sharing and the conventional SoC-based power-sharing methods. The results obtained show that the proposed power-sharing control significantly improves the light load efficiency compared to the conventional and equal power sharing methods. At high loads, the proposed method gives a higher efficiency than the SoC-based method, and an equivalent efficiency to the equal power-sharing method.**

Index Terms**-- Battery Management Systems, Efficiency Improvement, Modular Battery Energy Storage System**

I. INTRODUCTION

THE deployment of battery energy storage systems (BESSs) is increasing rapidly due to the increased integration of renewable energy systems and electric vehicles. BESSs are used for various purposes, such as providing a standalone power source for electric vehicles and maintaining power balance in standalone renewable energy systems. They are also used for supplying critical loads during power outages, peak shaving, power fluctuation mitigation, and ramp rate control in grid-connected systems [1, 2]. To ensure reliable operation, safety, and a prolonged battery lifespan of BESSs, an appropriate battery management system (BMS) is normally used. The BMS monitors the voltage, current, and temperature, and estimates the state of charge (SoC) of the individual battery cells [3]. If a predefined limit of one of these parameters is reached for one cell in a series string, the BMS stops the charging/discharging process, regardless of the status of the other cells in the string. This is to prevent overcharging/deep-discharging, and it consequently improves the battery's lifespan. However, this also reduces the effective overall capacity, due to under-utilization of the other cells' available capacity, if no balancing is performed for this series string.

Many different balancing methods have been proposed in the literature. A cheap and simple method is dissipative balancing, where the excess energy removed from higher charged cells is dissipated through a resistor [4]. In addition to wasting the available stored energy, the balancing current in this method is limited to several mA to prevent excessive heat generation, resulting in slow balancing. To improve the balancing efficiency, other methods utilize passive components to transfer energy from the higher charged cells to the lower ones. The switched capacitor energy transferring method [5] is simple and does not require closed loop control. However, energy transfer is only possible between adjacent cells, resulting in a long balancing time and low efficiency, especially in long strings. The chain structure method proposed in [6] increases the balancing speed, but energy transfer is still only possible between adjacent cells. A star connected switched capacitor balancing method that transfers energy from any cell to any other cell is proposed in [7]. However, capacitor based balancing methods balance voltages rather than SoC, resulting in low balancing speeds due to the flat discharge curves of batteries. Similarly, multi-inductor balancing [8] allows energy transfer between adjacent cells, but this also suffers from the slow balancing and low efficiency. The single inductor [9], and multi-winding transformer [10] methods allow energy exchange between arbitrary cells. However, the presence of diodes in the balancing paths limits the efficiency due to their power dissipation [11]. A symmetrical multi-winding transformer for direct cell-to-cell energy transfer is proposed in [11, 12]. Nevertheless, their design complexity increases with the number of cells in the battery string.

The battery packs used in a typical dc coupled microgrid [13] form a string of numerous series connected cells, allowing the battery voltage to match the dc bus.

This work is funded by the Turkish Ministry of National Education (Corresponding author: Bortecene Yildirim).

The authors are with the Electrical Power Research Group, School of Engineering, Newcastle University, Newcastle Upon Tyne NE1 7RU, U.K. (e-mail:y.bortecene2@ncl.ac.uk;mohammed.elgendy@ncl.ac.uk;andrew.smith@ncl.ac.uk; volker.pickert@ncl.ac.uk).

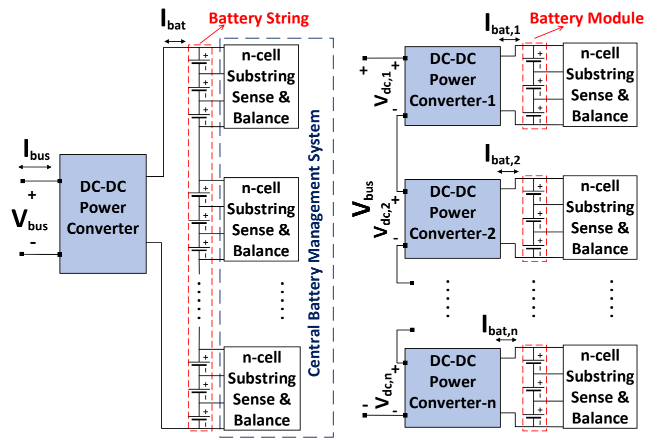

(a) Central converter based BESS (b) Modular BESS

Fig. 1. Structure of Battery Energy Storage System

A single dc-dc converter is used to control charging/discharging power of the string as shown in Fig. 1a. In this application, using the previously mentioned cell balancing methods, the cell equalization time, power loss, and/or design complexity increases with increased string length. For this reason, modular battery energy storage systems (MBESSs) with balancing functionality (Fig.1b) have been proposed [14-16]. In these modular systems, the power electronic converters are connected in series at the dc-bus side. This reduces the converter voltage ratings, allows independent connection of the battery modules, and gives individual battery power control. In addition, the lower battery string voltages allow better management of the battery cells with simpler cell balancing methods. The module bypassing capability of this system also improves the reliability further, as any faulty module(s) can be bypassed.

In the literature, different power sharing algorithms have been proposed for MBESSs. Huang et al [15], and Rehman et al [16] bring the system down to the cell level, removing the need for additional balancing circuits. SoC-based power sharing controllers balance the SoC of each cell during charging and discharging, along with the regulation of the dc bus voltage and battery power [17]. The ability to individually control batteries, and the degree of freedom of power sharing allowed by MBESSs, allows the use of different battery types, including recycled batteries. Considering these abilities, power sharing controllers have been proposed for pre-used batteries [18], hybrid batteries [19], and pre-used hybrid batteries [20].

In MBESSs, the converters are designed to process the full power of the battery modules, but they may operate at different power levels, depending on the power sharing and power demands. The power sharing controllers available in the literature are aimed at specific targets. For example, in the SoC-based power sharing [15, 16], the aim of the controller is to balance the SoC of each module while processing the battery power. This implies operating the modules at different powers depending on the SoC status of each module. In a similar manner, to utilize pre-used battery modules in MBESSs, different loading conditions for the individual battery modules are used depending on their state of health (SoH) [20]. In these cases, because the efficiencies of the converter modules depend on their loading, the overall energy conversion may be compromised. Indeed, the control flexibility of MBESSs opens the door to improving the system conversion efficiency while achieving the other control targets like SoC balancing. However, none of the available power sharing methods made use of the power control flexibility of the MBESS in improving the overall energy conversion efficiency of the system.

In this paper, an efficiency-based optimized power sharing method is proposed, along with the SoC management loop, and analyzed for the MBESS. This method is considering the effect of different power sharing ratios and battery power levels on the overall MBESS efficiency, based on the efficiencies of individual converters. An off-line Genetic Algorithm (GA) optimization is used to determine the power sharing ratios at different loads based on the system constraints. To deal with fast changes in battery load, a lookup table, generated based on the GA optimization, is used for real time implementation. In addition, an SoC management algorithm is implemented to ensure the modules SoC is always close to each other.

This paper is organized as follows. In Section II, the operational range and limitations of MBESSs are discussed, and the MBESS conversion efficiency is analyzed at different power levels and power sharing ratios. Section III formulates the optimization problem, and Section IV presents the implementation of the proposed real time efficiency optimized controller. The proposed optimized control method is experimentally verified and compared with the classical SoC power sharing method in Section V. Finally, Section VI concludes this paper.

II. Conversion Efficiency of Modular Converter

The power losses in the MBESS consist mainly of battery loss and converter loss. Overall loss minimization has been studied in [21] to determine the optimum charging strategy of a central Li-Ion battery for an EV application. The results show that the dominant loss of the system is the converter loss. This is because the internal resistances of batteries are small for low voltage battery packs, and therefore this has little impact on the total energy conversion efficiency compared to the converter losses. In MBESSs, lower voltage battery packs are mostly preferred, and therefore this paper will ignore the battery losses and focus only on the converter losses in the overall efficiency optimization of the system.

To understand the effect of the different power sharing ratios on the module efficiencies, a single converter from Fig. 1b, was analyzed at different power and voltage levels, with its efficiency map generated. It is worth mentioning that even if identical components are used for each converter in the MBESS, there may be slight parameter differences due to component tolerances. This may slightly affect the solution of the optimization problem. In this paper, for simplicity, the module converters are assumed identical, neglecting the parameter variations.

A bi-directional half bridge Buck-Boost converter was

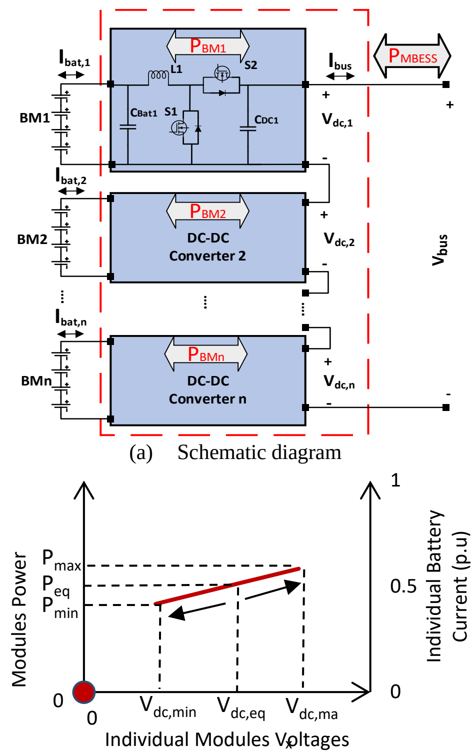

(a) Schematic diagram

(b) Operational Range of a Single Converter in MBESS

Fig. 2. The Modular Battery Energy Storage System

implemented for this system (Fig. 2a), and the following approach can also be used for optimization with other types of converters. It is assumed that the total MBESS battery power is shared amongst all active modules, and since the converter modules are connected in series, and share the same current at the dc bus side, each modules power (P_x) is directly proportional to its voltage at the series connected side ($V_{dc,x}$). This can be estimated from (1) for a given total battery power (P_{bat}).

$$P_x = \frac{V_{dc,x}}{V_{bus}} \times P_{bat} \tag{1}$$

The bus side voltage of each active converter module ranges between a minimum and a maximum value, as shown in Fig. 2b. Unless it is bypassed, the minimum voltage ($V_{dc,min}$) is equal to the battery voltage, and the maximum voltage ($V_{dc,max}$) depends on the voltage rating of the converter and the maximum duty ratio. When a module is bypassed, the active modules` dc bus side voltages, and hence power, increase to compensate for the resultant voltage and capacity drop.

A. Efficiency Map of a Single Converter Module

The main energy loss components of a power electronic converter are the conduction and switching losses. The two MOSFET switches employed in the Buck-Boost converter operate in the complementary mode. Their conduction losses ($P_{con,S1}$, $P_{con,S2}$) can be calculated from (2) and (3). The inductor conduction loss (P_L), in the continuous conduction mode, can be calculated from (4), whilst the RMS current ($I_{bat,rms}$) is calculated from (5) [22].

$$P_{con,S1} = I_{bat,rms}^2 \times R_{ds,on} \times d \tag{2}$$

$$P_{con,S2} = I_{bat,rms}^2 \times R_{ds,on} \times (1-d) \tag{3}$$

$$P_L = I_{bat,rms}^2 \times DCR \tag{4}$$

$$I_{bat,rms} = \sqrt{I_{bat}^2 + \frac{I_{ripple}^2}{12}} \tag{5}$$

where, $R_{ds,on}$ is the on-state resistance of MOSFET, and d is the duty ratio, and DCR and I_{ripple} are the equivalent dc resistance and ripple current of the inductor, respectively.

The switching losses of the MOSFET are the sum of the voltage and current overlap loss (P_{V-I}) during switching, the diode dead-time loss (P_{dt}), diode reverse recovery loss (P_{rr}), MOSFET output capacitance loss ($P_{COSS,FET}$), and the gate charge loss (P_G). These can be calculated from (6)-(10).

$$P_{V-I} = \frac{(V_{dc} + V_{DS,F}) \times I_{bat}}{2} \times f_{sw} \times (t_r + t_f) \tag{6}$$

$$P_{dt} = V_{SD} \times I_{bat} \times f_{sw} \times (t_{dtr} + t_{dtf}) \tag{7}$$

$$P_{rr} = Q_{RR} \times V_{dc} \times f_{sw} \tag{8}$$

$$P_{COSS,FET} = C_{OSS} \times V_{dc}^2 \times f_{sw} \tag{9}$$

$$P_G = (Q_{g1} + Q_{g2}) \times V_{GS} \times f_{sw} \tag{10}$$

where V_{dc} and V_{GS} represent the dc bus side and gate-source voltages, f_{sw} is the switching frequency, t_r and t_f are the rise and fall times of the switching transitions, and t_{dt1} and t_{dt2} are the dead times. C_{OSS} and Q_g are the MOSFET's output capacitance and total gate charge, and Q_{RR} represents the diode reverse recovery charge.

The converter loss (P_C), is the sum of the individual loss components (11), and the converter efficiency (η_c) can be calculated using (12) at different battery power and voltage levels.

$$P_C = P_{con,s1} + P_{con,s2} + P_L + P_{V-I} + P_{dt} + P_{rr} + P_{COSS} + P_G \tag{11}$$

$$\eta_c(\%) = \frac{P_{in} - P_C}{P_{in}} \times 100\% \tag{12}$$

The converter efficiencies are calculated for a switching frequency of 250 kHz, assuming a 12.8 V battery, dc bus voltages between 12.8 V and 40 V, and currents from 0 to 10 A. The Boost and Buck mode converter efficiencies are shown in Figs. 3a and 3b, respectively. In both cases, low converter efficiency occurs at light load due to the higher contribution of the switching losses, with a peak efficiency occurring around 30% load. After the peak efficiency point, it starts to decrease slightly because of the quadratic relationship between the conduction losses and the current.

B. System Conversion Efficiency

The MBESS system conversion efficiency can be estimated

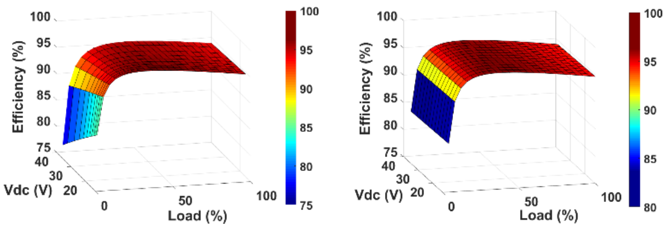

(a) Discharging (Boost) mode (b) Charging (Buck) mode

Fig. 3. The efficiency of the half-bridge converter

using (13). The effect of the individual converter efficiency (η_x) on the total system efficiency (η_s) is directly proportional to its share of the total power. As the current at the series connected side is the same for all modules, the power weighting factor (w_x) of an individual module is directly proportional to its dc bus side voltage (14).

$$\eta_s = \sum_{x=1}^{n} \eta_x \times w_x \tag{13}$$

$$w_x = \frac{V_{dc,X}}{V_{bus}} \tag{14}$$

III. Problem Formulation & Optimization

In this paper, an offline GA is used to optimize the power sharing ratios of the active modules based on the efficiency map of the converter and operating powers of the modules. The objective is to minimize the total system conversion loss as defined in (15), considering the loss components of the individual converters represented in (11). Offline optimization is considered because the loss component calculations depend on some component parameters that are not easy to measure online. These include the rise and fall times of switching transitions and the MOSFET's output capacitance and total gate charge. However, advances in the parameter identification of power electronic devices/converters may make online optimization possible in the future.

$$\min .\, fobj = \sum_{x=1}^{n} P_{C,x} \tag{15}$$

There is a tradeoff between the accuracy and the required time and memory size for the calculation of the optimization problem. As an offline algorithm is used in this paper, the main concern is the accuracy of the solution. Therefore, a relatively large population size of 400 was chosen to increase the accuracy of the optimum solution.

The sum of the module voltages is equal to the dc bus voltage (16). In order to limit degradation of the battery, the charge/discharge current is limited to 5A/10A respectively. These are the maximum continuous battery charge and discharge currents stated in the battery datasheet. The system parameters and limitations for this optimization are summarized in Table I.

$$\sum_{x=1}^{n} V_{dc,x} = V_{bus} \tag{16}$$

$$V_{dc,min} \le \{V_{dc,1}, V_{dc,2}, \dots, V_{dc,n}\} \le V_{dc,max} \tag{17}$$

$$0 \le \{I_{bat,1}, I_{bat,2}, \dots, I_{bat,n}\} \le I_{bat,max} \tag{18}$$

TABLE I

System Parameters

	System Parameters	Value
	Number of Modules, n	6
	dc Bus Voltage, V_{bus} (V)	120
	Discharging Power, $P_{s,d}$ (W)	768
	Charging Power, $P_{s,c}$ (W)	384
Battery	Rated Voltage, V_{Bat} (V)	12.8
	Capacity, C, (Ah)	10
	Maximum Continuous Discharge Current, $I_{bat,max}$ (A)	10
	Maximum Continuous Charge Current, $I_{bat,max}$ (A)	5
Converter	Maximum Voltage, $V_{dc,max}$ (V)	40
	Minimum dc Bus Side Voltage, $V_{dc,min}$ (V)	0/12.8
	Current Ratings, (A)	10
	Maximum duty ratio, d_{max}	0.8

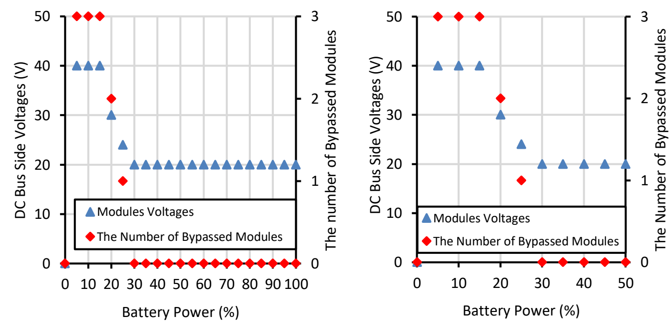

(a) Discharging mode (b) Charging mode

Fig. 4. The power allocation and bypassed modules

$$0 \le \{d_1, d_2, \dots, d_n\} \le d_{max} \tag{19}$$

The dc bus side converter voltages are the decision variables. The optimization algorithm is run from 0% to 100% load in 5% steps to generate the lookup table used in the practical implementation. A smaller step size would increase the accuracy, but at the expense of an enlarged lookup table, and consequently increased memory requirements.

The GA considers all possible operating points to find the minimum system loss within the system constraints using the equations from (2) to (19). Figures 4a and 4b show how the module voltages vary depending on the number of bypassed module(s) and load used, with Fig. 4a showing discharging mode, and Fig. 4b charging mode. Due to the continuous battery current charging limit, the maximum operation of the converter is half of its rated power in this mode. The results show that at light load, as many modules as possible should be bypassed to enable the operation at the modules' peak efficiency. However, this is normally restricted by the converter voltage ratings. As shown in Figs. 4a and 4b, with up to 15% load, 3 modules are bypassed, and the rest of the modules operate at their highest load. At 20% load 2 modules are bypassed, and at 25 % load only 1 module is bypassed. After the peak efficiency points, all modules are active and the power is evenly shared for the minimum system conversion loss.

IV. Real-Time Implementation

The implementations of the proposed efficiency-based power sharing method and the conventional SoC-based power sharing method are discussed in this section. In the SoC-based power sharing controller, there are two cascaded control loops [15] to balance the SoCs while regulating the dc bus voltage and battery power. The outer SoC balancing loop, shown in Fig. 5a, is common for both discharging and charging modes. This generates correction values, α_{v1} to α_{vn}, for each module based on the module`s relative SoC $(SoC_x - SoC_{avg})$. The initial correction values are zeros. When the module`s relative SoC is positive, i.e., the module has a higher SoC than the average value, its corresponding correction value will be positive, and vice versa. The reference dc bus side voltage of each module, $V_{dc,ref1}$ to $V_{dc,refn}$, is then determined by adding/subtracting the corresponding correction value in discharging/charging mode, respectively. As the dc bus side current is the same for all modules, the module with a higher dc bus side voltage will be assigned a higher power. Therefore, modules with a higher SoC than the average will be discharged with higher powers, and vice versa. Conversely, the module will be charged with a higher battery power than that of the average when its relative SoC is negative, and vice versa. The sum of the α_{vx} parameters (M_v) is used to keep the dc bus voltage at the desired value, and the individual module voltages are regulated using the inner voltage controller.

Figures. 5b and 5c show the control in the discharging and charging modes, respectively. Two parameters have been added to the block diagram in Fig. 5a compared to the controller proposed in [15] to make the charging and discharging control loops (Figs. 5b and 5c) applicable to the proposed method. The first is the SoC balancing loop enabling/disabling parameter (Δ), and the second is the module's bypass/activate parameter (βx), which are both set at 1 for the SoC balancing case.

In the proposed power sharing controller, Fig. 5a is disabled by setting Δ= 0 which results in all α_{vx} values being zero, and consequently equal power sharing of the active modules occurs. In this case, the power sharing is achieved by determining the optimum settings of the βx parameters in Figs. 5b and 5c considering the total battery power and modules' SoC. A lookup table is used for real time implementation to ensure a fast response to battery power variations. The real-time execution of the GA may not be fast enough to respond to a rapid change in the battery powers, so optimum sharing may not be achieved. In the worst-case scenario, efficiency reduction or/and overloading may occur for some battery modules. This may happen if some module(s) stay in their bypassed state when the battery power suddenly increases from low to full power. Therefore, to avoid any time delays between the change in the battery power and the optimum power sharing results, and to protect the battery from possible overloading, an off-line optimization algorithm is used. In addition to the execution time limitation, online optimization requires parameters that are difficult to measure/estimate as discussed in Section III.

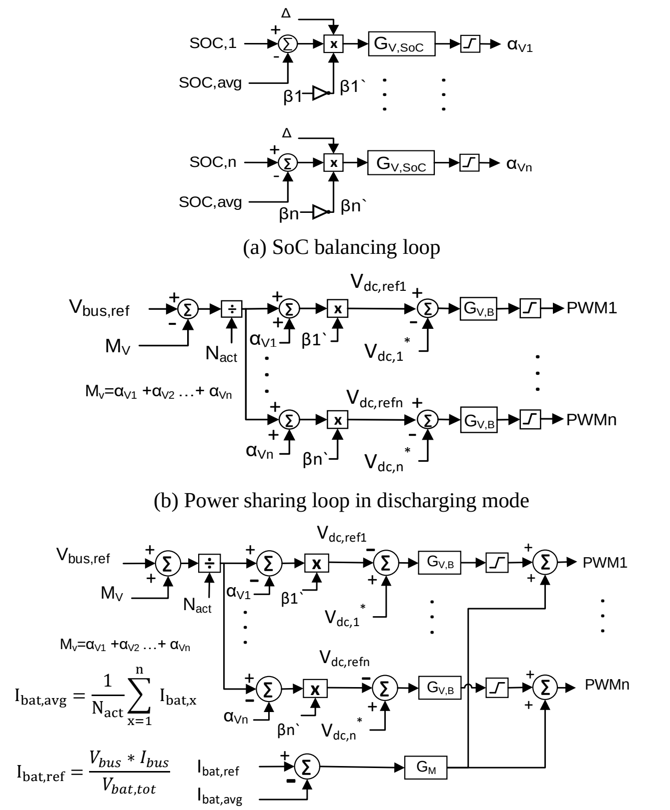

(a) SoC balancing loop

(b) Power sharing loop in discharging mode

(c) Power sharing loop in charging mode

Fig. 5. SoC-based power sharing controller

A simplified block diagram of the efficiency-based optimized power sharing controller is presented in Fig. 6a. In the off-line efficiency power sharing loop, the number of bypassed modules is determined using a lookup table. The input of the lookup table is the battery power, and six arbitrary bypass commands (β_{a1} to β_{a6}) are generated based on the optimization results. To bypass any module, its corresponding bypass command is set to 1, otherwise it is 0. Up to 15% battery power, β_{a1}, β_{a2}, and β_{a3} are set to 1, while the rest of the bypass commands are 0. At 20% battery power two commands (β_{a1} and β_{a2}) are set, while only β_{a1} is 1 at 25% battery power. The power sharing is then accomplished by the SoC management loop.

In the SoC management loop, the modules' SoCs are calculated using the coulomb counting method. When the SoH of battery reduces, calibration of capacity is necessary to accurately tracking the SoC of battery modules. and they are sorted in ascending order using the bubble sorting algorithm. Although the complexity of the bubble sorting algorithm increases with an increasing number of modules, it is easy to implement for the low number of modules considered in this study. After sorting the modules` SoCs, the modules to be bypassed, if any, are determined based on their relative SoC $(SoC_x - SoC_{avg})$, and the systems' mode of operation. Therefore, the bypass commands for the modules (β_1 to β_n) are determined within this loop. The reference dc bus side voltages of the modules are multiplied by the complementary signals of their associated bypass commands. When the bypass

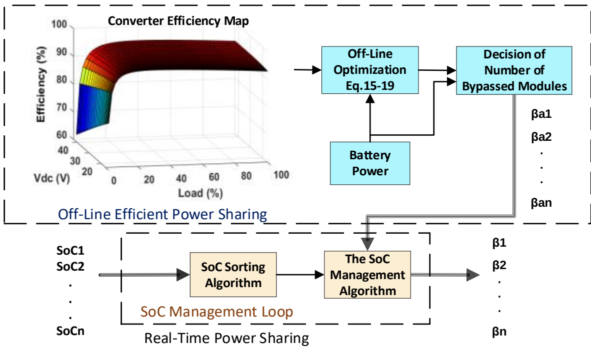

(a) Real-Time Implementation

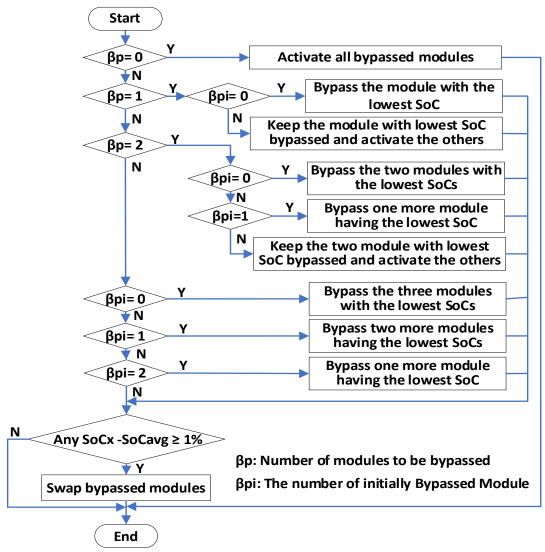

(b) SoC management algorithm in discharging mode

Fig.6. Proposed efficiency optimized power sharing

command for any module is 1, its reference dc bus side voltage will be 0, and the corresponding PWM is disabled.

A flowchart describing the SoC management control in the discharging case is shown in Fig. 6b. In this control, the module(s) with the lowest SoC are bypassed when bypass commands are generated. In MBESSs, although individual battery modules are not connected in series, it is important to keep their SoCs close to each other for better SoH degradation management. In the efficiency optimized power sharing proposed in this paper, a threshold limit of 1% deviation from the average SoC is chosen for the battery modules. A smaller limit will increase the swapping frequency of the bypassed modules. With SoH degradation, the effective capacity of the battery modules is reduced and consequently the swapping frequency of the bypassed modules is expected to increase. The SoCs of the bypassed modules are checked, and when any bypassed module`s relative SoC reaches 1% it will be reconnected, and the active module with the lowest SoC is then bypassed. When the number of bypassed modules changes, the previously bypassed modules are kept in their bypassed state as long as their relative SoCs are within the 1% limit. A similar flowchart can be created for the charging mode but in this case, bypassing of the higher SoC modules occurs.

TABLE II

EXPERIMENTAL SYSTEM PARAMETERS

System Parameters	Value	
	Discharging	**Charging**
Sampling Time (s)	1	1
Initial SoC of Battery-1 (%)	90	53
Initial SoC of Battery-2 (%)	88	54
Initial SoC of Battery-3 (%)	86	55
Initial SoC of Battery-4 (%)	87	53.5
Initial SoC of Battery-5 (%)	87.5	52
Initial SoC of Battery-6 (%)	89	52.5
Time (min)	**Battery Discharge-Power (%)**	**Battery Charge-Power (%)**
0-8	10	10
8-16	20	20
16-24	25	25
24-32	40	30
32-40	70	40
40-48	100	50

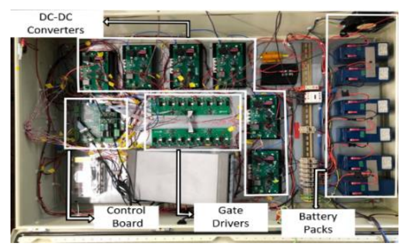

Fig. 7. Experimental 6-module MBESS System

V. EXPERIMENTAL RESULTS

The experimental setup which comprises of six LiFePo4 battery modules, and six half-bridge bidirectional dc-dc converters is shown in Fig. 7. The experimental systems parameters are listed in Table I while the test parameters are presented in Table II. The control system was implemented on a TMS320F28377d Texas Instruments digital signal processor (DSP). Both the SoC-based power sharing and the proposed power sharing controllers were tested in the charging and discharging modes, with different power and initial SoC mismatches. In discharging mode, the system was loaded with a dc electronic load connected to the dc bus, and the dc bus voltage was regulated to 120V by the MBESS. In charging mode, a dc power supply was connected to the dc bus to charge the battery modules at different power levels, with the power sharing achieved using the power sharing controller.

Figures. 8a and 8b present the experimental efficiency of a single half-bridge converter in the Boost and Buck operating modes. The input and output voltages and currents of the module were measured at specific charging/discharging currents and dc bus side voltages. In discharging mode, a single battery module was connected to the resistive load via a converter. The efficiency was then calculated using the input and output converter powers. For the discharging case, samples were taken at 1 A, 2 A, 4 A, 7 A, and 10 A battery currents, and 16 V, 20 V, 30 V, and 40 V dc bus side voltages.

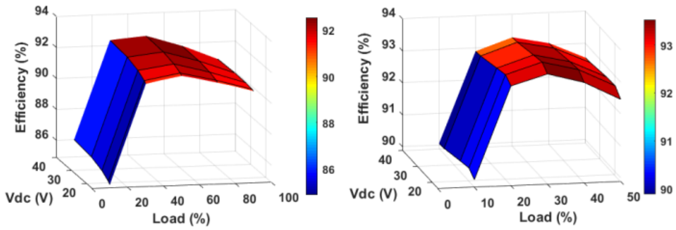

(a) Discharging (Boost) mode (b) Charging (Buck) mode

Fig. 8. The experimental efficiency of the half-bridge converter

For the charging case, the same dc bus side voltages were used, with battery currents of 1 A, 2 A, 3 A, 4 A, and 5A. The measured efficiency is slightly lower than that based on the datasheet values, with a peak efficiency of 93.1 % obtained in discharging mode, and 93.6 % in charging mode. Additional cable connections and parameter variations are contributing to the total losses in the practical system.

A. Discharging Mode

Results for the SoC-based power sharing controller in discharge mode are presented in Fig. 9 for the initial SoC values and battery discharging powers shown in Table II. Figure 9a shows the individual module voltages at the dc bus side. As the higher charged modules are being discharged with higher powers in discharging mode, Module 1, which has the greatest voltage and SoC, will be discharged the most, whilst Module 3, which has the lowest SoC, has the lowest discharge. Balancing is achieved based on the power difference of any module with respect to average value, which can be estimated at any time from (20). The balancing time depends on the initial SoC mismatches (ΔSoC_i), battery capacity (C), and power differences (21).

$$\Delta P(t) = I_{BUS(t)} \times (V_{dc,x(t)} - V_{dc,eq(t)}) \quad (20)$$

$$\Delta SoC_{(t)} = \Delta SoC_i - \frac{1}{C} \times \int_0^t (V_{dc,x(t)} - V_{dc,eq}) \times I_{BUS(t)} dt \quad (21)$$

When the battery power increases, the power difference increases, and faster equalization occurs. In this experiment, all modules are balanced after 35 minutes, after which the battery power is evenly shared as shown in Fig. 9d.

Results for the efficiency-based optimized power sharing controller in discharging mode are presented in Fig. 10. For this testing, the maximum number of bypassed modules was kept at 3 to not exceed the voltage rating of the active modules. Based on the optimized power sharing controller shown in Fig. 6, with the load requiring 10% of the systems battery power, the 3 modules with the lowest SoC are bypassed. In this case, the 3 active modules are each loaded at 20% (instead of loading the 6 modules at 10%). When the battery power is increased from 10% to 20% at 8 minutes, one additional module is activated, with each active module operating at 30% of their rated load. During this transition, Module 5 has the highest SoC amongst the 3 bypassed modules, so this module is activated. At around 10 minutes, the relative SoC of the bypassed Module 4 reaches the predefined turn on value, and it is activated to ensure it does not exceed the predefined SoC differences. At the same time, the module with the lowest SoC (Module 2) is bypassed. Similarly, different modules are bypassed at different times, with Modules 3 and 6, 6 and 1, and 1 and 5 swapping at around, 12, 18, and 23 minutes, respectively. Between 16 and 24 minutes, five modules support the dc bus voltage, each providing 30% of their active module power. After the peak efficiency point (24 minutes), all modules share the power evenly, and each module`s relative SoC difference is less than 1%, as shown in Fig. 10c.

The system efficiency with both control methods is calculated using (13) and is presented in Fig. 11a for the discharging mode. The efficiency with the equal power sharing method is also included to show the effect of the power sharing ratios on the system efficiency at different power levels. With the proposed efficiency-based power sharing control method, the system efficiency is increased by 5.05%, 1%, and 0.6% at 10%, 20%, 25% battery powers respectively, compared to the equal sharing method. In comparison to the SoC-based power sharing controller, higher efficiencies of 3.35%, 0.7%, and 0.2% are obtained with the optimized power sharing controller at 10%, 20% and 25% battery power respectively. It is worth mentioning that the power difference in the SoC-based power sharing controller depends on the SoC mismatch level. When all modules` SoC are equal, the modules share the power evenly, and the system conversion efficiency will be equal to the equal sharing case. Indeed, because of the continuous balancing with the SoC-based power sharing, the expected imbalance levels and power differences of the modules are very low. Thus, the modules operation is very close to the equal sharing case, restricting the light load efficiency improvement capability of the SoC-based power sharing.

The experimentally measured efficiencies with the SoC based power sharing and proposed efficiency-based power sharing control methods in discharging mode are included in Fig. 11b with 1 s sampling time. The results show that, when the SoC differences changes the system conversion efficiency varies with the SoC-based power sharing controller. Indeed, the system conversion efficiency reduces with the reduction in the SoC differences at 10%, 20% and 25% total battery power. Whilst, there is slight efficiency increase at 40%, and 70% battery power because of reduction in the level of SoC mismatches among the battery modules. Both the SoC-based and efficiency-based optimized power sharing controllers have the same system conversion efficiency at 100% battery power, as the power is shared evenly among the modules in both cases. There is a slight difference between the estimated and measured efficiencies as shown in Fig.11, which may be caused by nonlinear behavior of the circuit components and losses in the added wires. However, both analytical and experimental results verify the superiority of the proposed optimized power sharing controller. The proposed efficiency optimized controller has a higher system efficiency than that of the SoC-based power sharing controller at all battery powers. Compared to the efficiency of the SoC-based power sharing controller, the experimental efficiency is improved using the proposed controller by 2.6%, 0.5% and 0.15% at 10%, 20%, and 25% battery powers, respectively.

The full range of estimated system efficiencies for the SoC-based, efficiency-based, and equal power sharing controllers

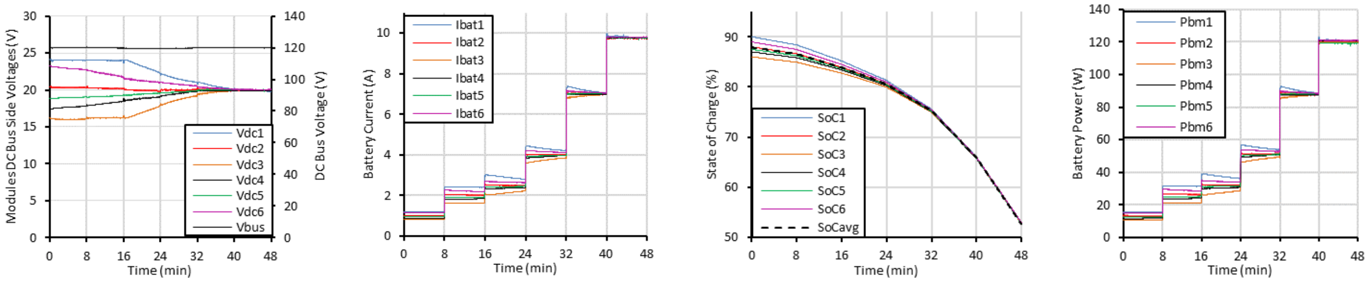

(a) Module dc bus side voltages b) Battery Currents (c) SoC (d) Individual Module Powers

Fig. 9. Experimental results with SoC-based power sharing controller in discharging mode

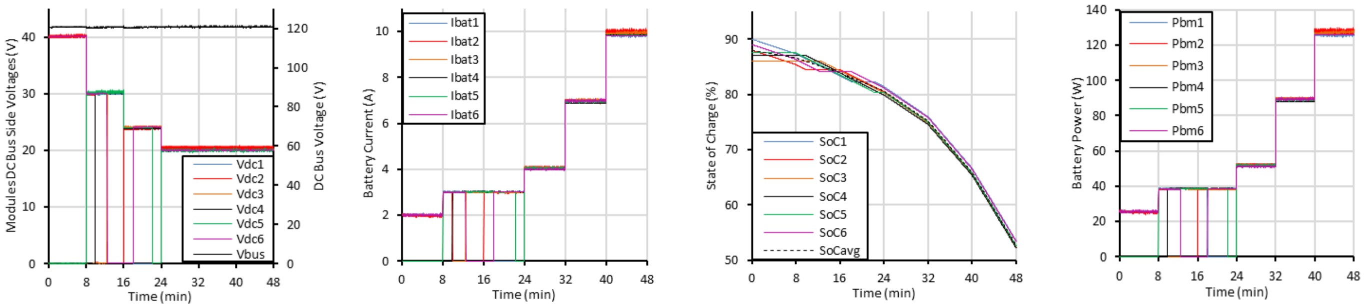

(a) Module dc bus side voltages (b) Battery Currents (c) SoC (d) Individual Module Powers

Fig. 10. Experimental results with efficiency-based power sharing controller in discharging mode

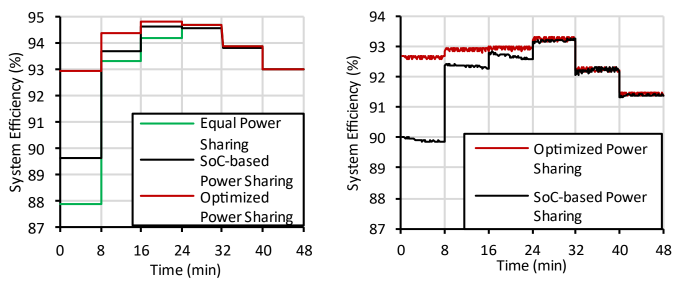

(a) Estimated efficiency (b) Experimental efficiency

Fig. 11. System Conversion Efficiency during discharging

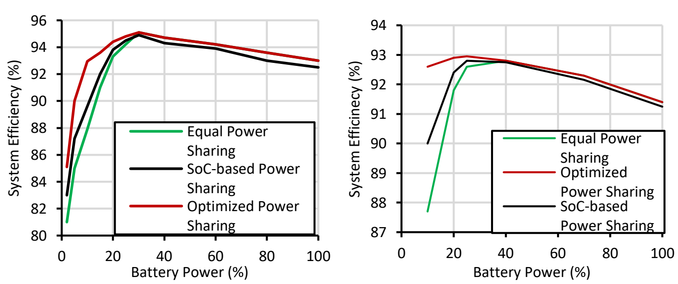

(a) Estimated efficiency (b) Experimental efficiency

Fig. 12. Discharging operational system efficiency at different loading

are shown in Fig. 12a for the discharging mode. The battery modules power differences in the SoC-based power sharing controller depends on the cell mismatch level. Therefore, when all cells are under balanced conditions, there will be no light load efficiency improvement with the SoC-based power sharing, and the conversion efficiency will be the same as the equal power sharing method. In addition, if there is SoC mismatch, the SoC-based controller has a lower system efficiency than that of the equal sharing case after the peak efficiency point, 28% of battery power in this case. This reduction is prevented if the optimized power sharing controller is used. The full range of measured system efficiencies are shown in Fig. 12b. Although, the measured efficiency is slightly lower than that of the estimated, the light load efficiency of the system is improved using the proposed optimized power sharing controller compared to the equal sharing case by 4.9%, 1.1%, and 0.35% at 10%, 20% and 25 % total battery powers, respectively. Both estimated and measured efficiency results validate the effectiveness of the proposed power sharing controller over the full load range of battery discharging.

B. Charging Mode

For charging mode, the initial module SoC and the battery charging powers, are shown in Table II. A dc power supply with a voltage of V_{bus} is connected to the dc bus to charge the batteries with the variable charging current. The SoC balancing and power distribution are accomplished by the power sharing control loop shown in Fig.5c. The results of the SoC-based power sharing controller and the proposed efficiency-based optimized power sharing controller are presented in Figs. 13 and 14, respectively. In comparison to the discharging mode, with the SoC-based power sharing controller, the higher charged modules are charged with lower powers, and vice versa. When the battery module SoCs converge, the dc bus side voltages also converge, as the modules relative SoC differences and correction values reduce. When all modules SoC are balanced, they share the power evenly. With the efficiency-based power sharing controller, the higher charged modules are bypassed if there is any bypass command.

Fig 15a. shows the estimated system efficiency with the SoC-based power sharing controller, optimized power sharing

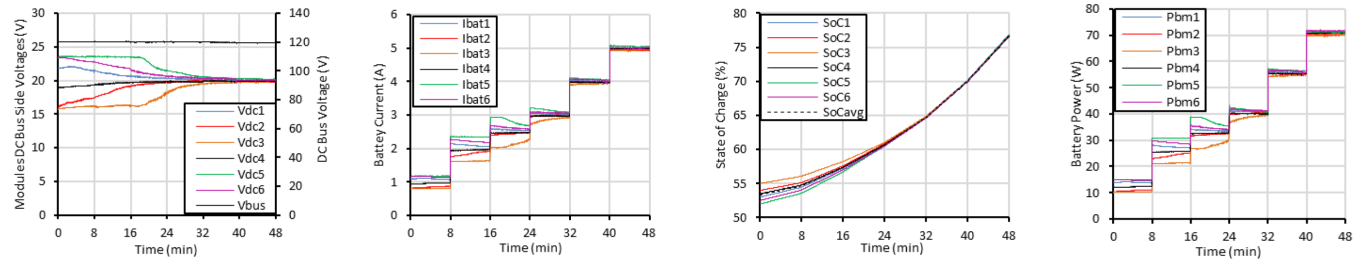

(a) Module dc bus side voltages (b) Battery Currents (c) SoC (d) Individual Module Powers

Fig. 13. Experimental results for the SoC-based power sharing controller in charging mode

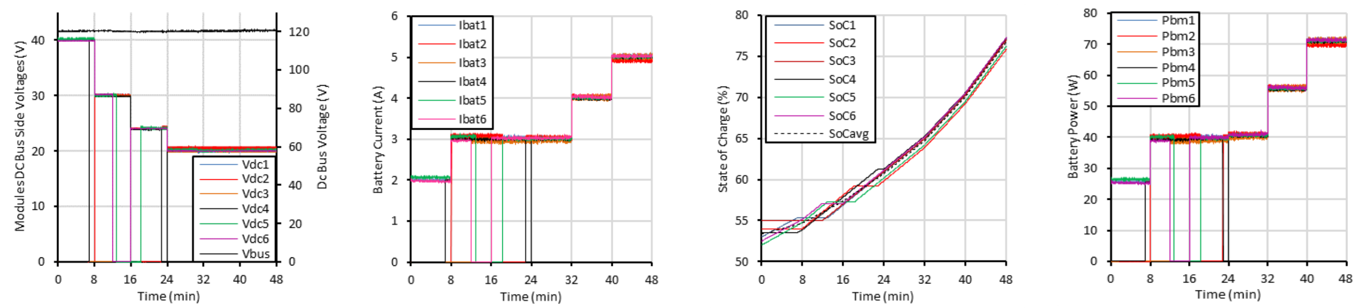

(a) Module dc bus side voltages (b) Battery Currents (c) SoC (d) Individual Module Powers

Fig. 14. Experimental results for the efficiency-based power sharing controller in charging mode

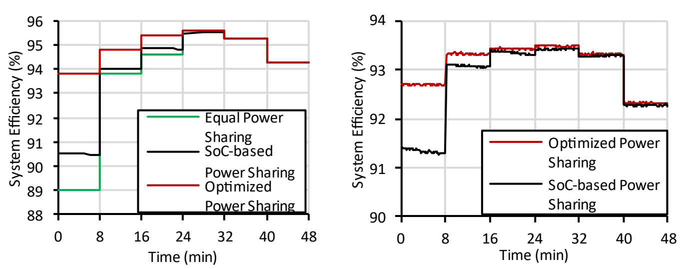

(a) Estimated efficiency (b) Experimental efficiency

Fig. 15. System Conversion Efficiency during charging

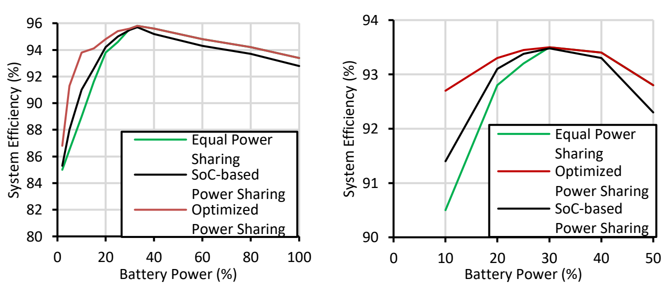

(a) Estimated efficiency (b) Experimental efficiency

Fig. 16. Charging operational system efficiency at full load range

controller, and equal power sharing method. A limited efficiency improvement of 1.5% is achieved at 10% load with the SoC-based power sharing controller compared to the equal power sharing case. On the other hand, up to a 4.8% efficiency improvement can be achieved with the efficiency optimized controller at the same battery power regardless of the cell mismatch level. The measured efficiency for the SoC-based power sharing and optimized power sharing controllers is shown in Fig. 15b. These results show that the optimized power sharing controller increases the system conversion efficiency compared to the SoC-based power sharing controller, by 1.3%, 0.2%, and 0.1% at 10%, 20%, and 25% battery powers, respectively.

The operational system efficiencies of the SoC-based, efficiency-based, and equal power sharing controllers are shown in Fig. 16 for the charging mode. In a similar way to the discharging case, the SoC-based power sharing controller efficiency varies between the SoC-based power sharing curve and equal power sharing curve depending on the mismatch level. On the other hand, the optimized power sharing controller has a higher charging efficiency at light load, and the same efficiency as the equal power sharing case at heavy load. When the modules operate with a very low SoC mismatch level, for a 10% battery power, the practical efficiency of the proposed power sharing controller is 2.7% higher than that of the SoC-based power sharing method. This is presented in Fig. 16b. Apart from the slight variations between the estimated and measured efficiencies, both results evidence the superiority of the proposed efficiency optimized power sharing controller.

VI. Conclusion

This article proposes an efficiency-based power sharing controller for an MBESS. The effect of power sharing ratios on the systems conversion efficiency is analyzed by considering a single converters efficiency. The results show that the light load efficiency is improved by up to 5.05 % with the proposed optimized controller without any additional components, by utilizing the bypassing ability of the MBESS. In addition, compared to the SoC-based power sharing controller, where the system efficiency reduces with mismatches after the peak efficiency point, the efficiency reduction is reduced with equal power sharing in the proposed method. Rather than keeping all of the modules SoCs at an equal state, this strategy keeps the SoC values very close to each other and improves the total system conversion efficiency.

VII. References

[1] T. T. Ku and C. S. Li, "Implementation of Battery Energy Storage System for an Island Microgrid with High PV Penetration," in *2020 IEEE/IAS 56th Industrial and Commercial Power Systems Technical Conference (I&CPS)*, 2020, pp. 1-8.

[2] H. Gong, V. Rallabandi, M. L. McIntyre, E. Hossain, and D. M. Ionel, "Peak Reduction and Long Term Load Forecasting for Large Residential Communities Including Smart Homes With Energy Storage," *IEEE Access*, vol. 9, pp. 19345-19355, 2021.

[3] R. Zhang, J. Wu, R. Wang, R. Yan, Y. Zhu, and X. He, "A Novel Battery Management System Architecture Based on an Isolated Power/Data Multiplexing Transmission Bus," *IEEE Transactions on Industrial Electronics*, vol. 66, no. 8, pp. 5979-5991, 2019.

[4] B. Yildirim, M. Elgendy, A. Smith, and V. Pickert, "Evaluation and Comparison of Battery Cell Balancing Methods," in *2019 IEEE PES Innovative Smart Grid Technologies Europe (ISGT-Europe)*, 2019, pp. 1-5.

[5] C. Pascual and P. T. Krein, "Switched capacitor system for automatic series battery equalization," in *Proceedings of APEC 97 - Applied Power Electronics Conference*, 1997, vol. 2, pp. 848-854 vol.2.

[6] M. Kim, C. Kim, J. Kim, and G. Moon, "A Chain Structure of Switched Capacitor for Improved Cell Balancing Speed of Lithium-Ion Batteries," *IEEE Transactions on Industrial Electronics*, vol. 61, no. 8, pp. 3989-3999, 2014.

[7] Y. Ye, K. W. E. Cheng, Y. C. Fong, X. Xue, and J. Lin, "Topology, Modeling, and Design of Switched-Capacitor-Based Cell Balancing Systems and Their Balancing Exploration," *IEEE Transactions on Power Electronics*, vol. 32, no. 6, pp. 4444-4454, 2017.

[8] T. H. Phung, J. Crebier, A. Chureau, A. Collet, and V. Nguyen, "Optimized structure for next-to-next balancing of series-connected lithium-ion cells," in *2011 Twenty-Sixth Annual IEEE Applied Power Electronics Conference and Exposition (APEC)*, 2011, pp. 1374-1381.

[9] S. Park, T. Kim, J. Park, G. Moon, and M. Yoon, "A New Buck-boost Type Battery Equalizer," in *2009 Twenty-Fourth Annual IEEE Applied Power Electronics Conference and Exposition*, 2009, pp. 1246-1250.

[10] N. H. Kutkut, H. L. N. Wiegman, D. M. Divan, and D. W. Novotny, "Design considerations for charge equalization of an electric vehicle battery system," *IEEE Transactions on Industry Applications*, vol. 35, no. 1, pp. 28-35, 1999.

[11] S. Li, C. C. Mi, and M. Zhang, "A High-Efficiency Active Battery-Balancing Circuit Using Multiwinding Transformer," *IEEE Transactions on Industry Applications*, vol. 49, no. 1, pp. 198-207, 2013.

[12] Y. Chen, X. Liu, Y. Cui, J. Zou, and S. Yang, "A MultiWinding Transformer Cell-to-Cell Active Equalization Method for Lithium-Ion Batteries With Reduced Number of Driving Circuits," *IEEE Transactions on Power Electronics*, vol. 31, no. 7, pp. 4916-4929, 2016.

[13] M. D. V, G. Bhuvaneswari, and B. Singh, "A Reliable Microgrid Comprising Solar PV-WEGS and Battery With Seamless Power Transfer Capability," *IEEE Transactions on Industrial Electronics*, vol. 68, no. 10, pp. 9665-9674, 2021.

[14] Y. Li and Y. Han, "A module-integrated distributed battery energy storage and management system," *IEEE Transactions on Power Electronics*, vol. 31, no. 12, pp. 8260-8270, 2016.

[15] W. Huang and J. A. A. Qahouq, "Energy Sharing Control Scheme for State-of-Charge Balancing of Distributed Battery Energy Storage System," *IEEE Transactions on Industrial Electronics*, vol. 62, no. 5, pp. 2764-2776, 2015.

[16] M. Muneeb Ur Rehman, "Modular, Scalable Battery Systems with Integrated Cell Balancing and DC Bus Power Processing," *Ph.D. dissertation, Utah State University*, 2018.

[17] S. Chowdhury, M. N. B. Shaheed, and Y. Sozer, "State-of-Charge Balancing Control for Modular Battery System With Output DC Bus Regulation," *IEEE Transactions on Transportation Electrification*, vol. 7, no. 4, pp. 2181-2193, 2021.

[18] Y. Li and Y. Han, "Used-battery management with integrated battery building block system," in *2015 IEEE Applied Power Electronics Conference and Exposition (APEC)*, 2015, pp. 3177-3182.

[19] N. Mukherjee and D. Strickland, "Control of Cascaded DC–DC Converter-Based Hybrid Battery Energy Storage Systems—Part I: Stability Issue," *IEEE Transactions on Industrial Electronics*, vol. 63, no. 4, pp. 2340-2349, 2016.

[20] N. Mukherjee and D. Strickland, "Analysis and Comparative Study of Different Converter Modes in Modular Second-Life Hybrid Battery Energy Storage Systems," *IEEE Journal of Emerging and Selected Topics in Power Electronics*, vol. 4, no. 2, pp. 547-563, 2016.

[21] Z. Chen, B. Xia, C. C. Mi, and R. Xiong, "Loss minimization-based charging strategy for lithium-ion battery," in *2014 IEEE Energy Conversion Congress and Exposition (ECCE)*, 2014, pp. 4306-4312.

[22] J. Depew, "Efficiency analysis of a synchronous buck converter using Microsoft® Office® Excel®-based loss calculator," *Microchip Technology Inc.*, pp. 1-14, 2012. [Online]. Available: http://ww1.microchip.com/downloads/en/Appnotes/01471A.pdf.

Bortecene Yildirim is currently pursuing the Ph.D. degree with Newcastle University, Newcastle Upon Tyne, U.K. He received an M.Sc. degree in Electrical Power from Newcastle University, UK in 2017 and B.Sc. in Electrical and Electronics Engineering from Middle East Technical University, Turkey, in 2013.

His research interests include battery management systems, and power electronic converters for renewable generation schemes.

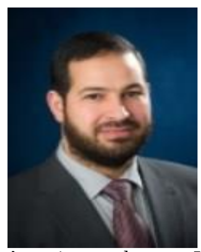

Mohammed A. Elgendy received the BSc degree from Menoufia University, Egypt, in 1997, the MSc degree from Ain Shams University, Egypt in 2003, and the PhD degree from Newcastle University, UK, in 2010, all in Electrical Engineering.

From June 1998 to May 2006, he was a Research Assistant at the New and Renewable Energy Department, Desert Research Centre, Cairo, Egypt. He joined the Electrical Power research group at Newcastle University in 2011 as a Research Associate and got a Lecturer position with the group in 2015. His current research focus is on the design and control of power electronic converters for renewable energy systems, battery energy storage systems, and electric drives.

Andrew N. Smith received the M.Eng. (Hons.) and Eng.D degrees in electrical and electronic engineering from Newcastle University, Newcastle upon Tyne, U.K., in 2002 and 2009, respectively.

He is currently a Lecturer with the Electrical Power Research Group, Newcastle University. His current research interests include the control of power converters, electric drives, and renewable energy systems.

Volker Pickert (Member, IEEE) studied at RWTH Aachen University, Aachen, Germany, and the University of Cambridge, Cambridge, U.K. He received the Dipl. Ing. degree in electrical and electronic engineering from RWTH Aachen University in 1994 and the Ph.D. degree in power electronics from Newcastle University, Newcastle upon Tyne, U.K., in 1997.

From 1998 to 1999, he was an Application Engineer with Semikron GmbH, Nuremberg, Germany. From 1999 to 2003, he was a Group Leader with Volkswagen AG, Wolfsburg, Germany, responsible for the development of electric drives for electric vehicles. In 2012, he became the Head of the Electrical Power Group and, in 2020, the Director of Discipline for Electrical and Electronic Engineering, Newcastle University. His current research interests include power electronics for transport applications, thermal management, health monitoring techniques, and advanced nonlinear control.

In 2019, Prof. Pickert became the Director of the U.K.'s EPSRC Doctoral Training Centre in Power Electronics for Sustainable Electric Propulsion. He is the active Editor-in-Chief of the IET Power Electronics journal.